THE JOURNAL OF BIOLOGICAL CHEMISTRY VOL. 290, NO. 48, pp. 28746–28759, November 27, 2015

Molecular Mechanisms and Kinetic Effects of FXYD1 and Phosphomimetic Mutants on Purified Human Na,K-ATPase*

Received for publication, August 26, 2015, and in revised form, September 24, 2015 Published, JBC Papers in Press, October 1, 2015, DOI 10.1074/jbc.M115.687913

Neeraj Kumar Mishra[‡], Michael Habeck[‡1], Corinna Kirchner[§], Haim Haviv[‡], Yoav Peleg[¶], Miriam Eisenstein[‖], Hans Juergen Apell[§], and Steven J. D. Karlish[‡1]

From the [‡]Department of Biological Chemistry, [‖]Department of Chemical Research Support, and [¶]Israel Structural Proteomics Center, Weizmann Institute of Science, Rehovot 7610001, Israel and the [§]Department of Biology, University of Konstanz, 78464 Konstanz, Germany

Background: FXYD1 regulates Na,K-ATPase in heart and other tissues.
Results: Purified human isoforms ($\alpha1\beta1$ and $\alpha2\beta1$) reconstituted with wild-type FXYD1 or phosphomimetic mutants S63E, S68E, and S63E,S68E provide detailed information on kinetic effects.
Conclusion: FXYD1 slows conformational transition E_2(2K)ATP → E_1(3Na)ATP and raises binding affinity to Na^+ site III.
Significance: A detailed picture emerges of the regulatory mechanism of FXYD1 that complements physiological studies.

Phospholemman (FXYD1) is a single-transmembrane protein regulator of Na,K-ATPase, expressed strongly in heart, skeletal muscle, and brain and phosphorylated by protein kinases A and C at Ser-68 and Ser-63, respectively. Binding of FXYD1 reduces Na,K-ATPase activity, and phosphorylation at Ser-68 or Ser-63 relieves the inhibition. Despite the accumulated information on physiological effects, whole cell studies provide only limited information on molecular mechanisms. As a complementary approach, we utilized purified human Na,K-ATPase ($\alpha1\beta1$ and $\alpha2\beta1$) reconstituted with FXYD1 or mutants S63E, S68E, and S63E,S68E that mimic phosphorylation at Ser-63 and Ser-68. Compared with control $\alpha1\beta1$, FXYD1 reduces V_{max} and turnover rate and raises $K_{0.5}$Na. The phosphomimetic mutants reverse these effects and reduce $K_{0.5}$Na below control $K_{0.5}$Na. Effects on $\alpha2\beta1$ are similar but smaller. Experiments in proteoliposomes reconstituted with $\alpha1\beta1$ show analogous effects of FXYD1 on $K_{0.5}$Na, which are abolished by phosphomimetic mutants and also by increasing mole fractions of DOPS in the proteoliposomes. Stopped-flow experiments using the dye RH421 show that FXYD1 slows the conformational transition E_2(2K)ATP → E_1(3Na)ATP but does not affect 3NaE_1P → E_2P3Na. This regulatory effect is explained simply by molecular modeling, which indicates that a cytoplasmic helix (residues 60–70) docks between the αN and αP domains in the E_2 conformation, but docking is weaker in E_1 (also for phosphomimetic mutants). Taken together with previous work showing that FXYD1 also raises binding affinity for the Na^+-selective site III, these results provide a rather comprehensive picture of the regulatory mechanism of FXYD1 that complements the physiological studies.

Animal cells need an inwardly directed Na^+ concentration gradient and an outwardly directed gradient for K^+ ions in order to maintain viability. Numerous cellular functions depend on the presence of these electrochemical potential gradients; therefore, a strict regulation is required. The K^+ gradient preferentially controls the electric membrane potential, and the Na^+ gradient is required to fuel a variety of coupled transporters, such as the uptake of sugars, amino acids, or phosphate and the extrusion of Ca^{2+} at the expense of a Na^+ influx into the cells. The primary actor maintaining the cation gradients is the Na,K-ATPase. Because the demand for the ion pump capacity differs widely between various types of cells, four α and three β isoforms are expressed and assembled as complexes at appropriately adapted densities in the various cell membranes (1). In addition, in specific tissues, such as excitable cells or kidney, the Na^+ extrusion and K^+ uptake capacity must be modulated acutely. For this purpose, a third, regulatory subunit, has evolved, and these subunits are referred to as the FXYD family (2–4). FXYD proteins are a group of seven short, single-transmembrane proteins named after the invariant extracellular motif F*X*YD (5). The molecular mechanism of the regulatory effects of these FXYD proteins is still under investigation. Many years before its function was revealed, FXYD1 (known also as phopholemman) was identified as the major substrate for PKA and PKC in the heart (6, 7).

FXYD1 is a member of the family and is expressed prominently in heart and skeletal muscle and the brain (8, 9). According to NMR-spectroscopic investigations of purified FXYD1 in SDS-detergent micelles, the molecule is organized into four α-helices. H1 (Asp-12 to Gln-17) is located at the extracellular side; H2 (Ile-19 to Leu-36) forms the transmembrane domain; and the cytoplasmic domain contains two helices, H3 (Ser-37 to Lys-43) and H4 (Thr-59 to Ser-68) (10). Whereas helices H1, H2, and H3 are rigidly connected, H4 is linked to the others by a long and highly flexible loop. The high mobility of the C-terminal domain of all FXYD proteins, which contains H4 in FXYD1, is reflected in the fact that it is not resolved in any of the x-ray structures of crystallized Na,K-ATPase complexes containing FXYD2 and FXYD10, respectively (11, 12).

* This work was supported by the German-Israeli Foundation for Science and Development Grant 922-165.9 (to H.-J. A. and S. J. K.). The Israel Structural Proteomics Center is supported by the Dana and Yossie Hollander Center for Structural Biology. The authors declare that they have no conflicts of interest with the contents of this article.
[1] Supported by the Minerva Foundation.
[2] To whom correspondence should be addressed. Tel.: 972-8-934-2278; Fax: 972-8-934-4118; E-mail: Steven.Karlish@weizmann.ac.il.

In order to modulate the Na,K-ATPase activity in the short term, cells must be able to rapidly switch the regulatory function on and off. This switching function is largely attributable to the phosphorylation of FXYD1 by PKA and PKC. It has been found that this process occurs *in vivo* at residues Ser-63, Ser-68, and Thr-69, which are located in helix H4 (6, 13, 14). Numerous studies have provided evidence that FXYD1 phosphorylation raises the apparent affinity of the Na,K-ATPase for Na^+ ions in cardiac myocytes (15–17) and in heterologous expression systems (18–20) (reviewed in Ref. 21).

At a mechanistic level, the transduction of the regulatory information may occur at two different locations: (*a*) via the close contact of the transmembrane helix H2 of FXYD1 and helix TM9[3] of the α subunit of Na,K-ATPase (12) and (*b*) by direct interaction of the C-terminal helix H4 of FXYD1 with the cytoplasmic domain of the Na,K-ATPase. The interaction of the transmembrane helices has been proven in detergent-solubilized isolated complexes and in native cell membrane and is important for maintaining stability of the protein (22, 23). In recent studies, it has been shown that the charge of the cytoplasmic domain plays an important role in the regulation of the Na,K-ATPase (24). The strongly positively charged H4 helix of FXYD1 is assumed to adhere to a negatively charged region in the cytoplasmic domain of the Na,K-ATPase when unphosphorylated. Upon phosphorylation, negative charges are deposited on the surface of H4 of FXYD1, and it has been proposed that this modification will substantially weaken the attachment to the cytoplasmic domain of the Na,K-ATPase and thus affect the pump function (21).

The current study was performed in order to gain deeper insight into the kinetic mechanism and regulatory function of FXYD1. The experimental investigations were performed with complexes of isolated and reconstituted purified human α1His_{10}-β1 and α2His_{10}-β1 isoforms of the Na,K-ATPase expressed in *Pichia pastoris* and purified human FXYD1 and three phosphomimetic mutants, S63E, S68E, and S63E,S68E, expressed in *Escherichia coli*. Fluorescence techniques using the electrochromic shift dye RH421 were applied to obtain information on rates of conformational changes and electrogenic Na^+ binding (25) and a voltage-sensitive dye, 1,5-bis-(5-oxo-3-propylisoxazol-4-yl)-pentamethine oxonol (oxonol VI), to detect pump currents across reconstituted proteoliposome membranes (26). Computational docking studies reveal mechanistic concepts on a molecular level that allow a consistent explanation of the results. Overall, the results are consistent with the predominant current hypothesis of FXYD1 regulation of Na,K-ATPase (21) and add novel insights into the molecular mechanisms of functional and regulatory effects of FXYD1.

[3] The abbreviations used are: TM, transmembrane helix; DDM, *n*-dodecyl-β-maltoside; DOPS, 1,2-dioleoyl-*sn*-glycero-3-phospho-L-serine; DOPE, 1,2-dioleoyl-*sn*-glycero-3-phosphoethanolamine; DPPC, 1,2-dipalmitoyl-*sn*-glycero-3-phosphocholine; oxonol VI, bis-(3-propyl-5-oxoisoxazol-4-yl) pentamethine oxonol; RH421, *N*-(4-sulfobutyl)-4-(4-(4-(dipentylamino) phenyl) butadienyl)pyridinium; GEH, geometric-electrostatic-hydrophobic; Tricine, *N*-[2-hydroxy-1,1-bis(hydroxymethyl)ethyl]glycine; SOPS, 1-stearoyl-2-oleoyl-*sn*-glycero-3-phospho-l-serine; SOPC, 1-stearoyl-2-oleoyl-*sn*-glycero-3-phosphocholine.

Experimental Procedures

Materials

n-Dodecyl-β-maltoside (DDM) was purchased from Anatrace, and BD-Talon metal affinity resin was from Clontech. Soy phosphatidylcholine, 1,2-dioleoyl-*sn*-glycero-3-phospho-L-serine (DOPS), 1,2-dipalmitoyl-*sn*-glycero-3-phosphocholine (DPPC), and 1,2-dioleoyl-*sn*-glycero-3-phosphoethanolamine (DOPE) were purchased from Avanti Polar Lipids. AcTEV™ protease was from Life Technologies. ATP (disodium salt, special quality) was obtained from Roche Applied Science. The membrane potential-sensitive fluorescent dye oxonol VI and *N*-(4-sulfobutyl)-4-(4-(4-(dipentylamino)phenyl) butadienyl)pyridinium (RH421) were ordered from MoBiTec. Recombinant PKA (2,500,000 units/ml, catalog no. P6000L) was obtained from New England Biolabs. All other reagents were purchased from Merck or Sigma-Aldrich at the highest quality level available.

Methods

Recombinant Human Na,K-ATPase Expression and Purification—P. pastoris transformation, yeast growth, membrane preparation, and His tag purification of recombinant human α1β1FXYD1 and α2β1FXYD1 Na,K-ATPase were done essentially as described previously (27–30). Purified detergent-soluble Na,K-ATPase complexes were eluted from BD-Talon beads in a medium containing 250 mM imidazole, pH 7.2, 10% glycerol, 100 mM NaCl, 25 mM Tris-Tricine, pH 7.4, 0.12 mg/ml $C_{12}E_8$, 0.025 mg/ml cholesterol, 0.075 mg/ml SOPS, and 0.075 mg/ml SOPC. For stopped-flow measurements, the enzyme was eluted from BD-Talon beads in a medium containing 20 mM Na^+ and all other components as above. For steady-state Na,K-ATPase measurements, the enzyme was usually prepared in batch mode (specific activities 15–25 μmol/min/mg protein), whereas a gravity column-purified enzyme was used for stopped-flow kinetic measurements (specific activities 22–30 μmol/min/mg protein). For the turnover measurements in Table 3, the enzyme was prepared as described previously (29) in an elution buffer containing 100 mM NaCl, 30 mM imidazole, 10% glycerol, 20 mM MOPS/Tris, pH 7.4, 0.3 mg/ml C12 E8, 0.05 mg/ml cholesterol, 0.07 mg/ml SOPS plus 0.1 mg/ml soy phosphatidylcholine (specific activities 30–40 μmol/min/mg protein).

FXYD1 Mutants—Mutations were introduced into the wild-type hFXYD1 gene cloned into the expression vector pET28-TevH (23). Mutagenesis was performed using a transfer-PCR platform (31, 32). For the transfer-PCRs, each of the mutagenic primers was used in combination with PetRev primer (Table 1). Introduction of the mutations and the integrity of the entire protein open reading frame were verified by DNA sequencing. Reaction conditions and DNA amplification reactions were performed as described previously (31, 32).

Recombinant Human FXYD1 Expression, Purification, and Reconstitution—Human FXYD1 (phospholemman) and its three mutants, S63E, S68E, and the double mutant S63E,S68E, were expressed in *E. coli* CD41 cells from the pET28-TevH vector, as described for wild-type FXYD1 elsewhere (23, 30). FXYD1 purification has been described in detail (23, 30). For

TABLE 1
Primers used for transfer-PCR mutagenesis
Positions of the replacements in the different mutagenic primers are underlined.

Mutations	Primer name	Primer sequence (5′–3′)
S63E	TPhPLMS63EF	GAGGGAACTTTCCGCAGCGAAATCCGCCGTCTGTCC
S68E	TPhPLMS68EF	GCTCCATCCGCCGTCTGGAAACCCGCAGGCGGTAGGCG
S63E,S68E	TPhPLMS63_68EF	GAGGGAACTTTCCGCAGCGAAATCCGCCGTCTGGAAACCCGCAGGCGGTAGGCG
	PetRev	ATGCTAGTTATTGCTCAGCGGT

reconstitution with the Na,K-ATPase, FXYD1 was dialyzed against 500 mM NaCl, 10% glycerol, 0.1 mM DTT, and 25 mM MOPS, pH 7.4, and the His tag was removed by AcTev-protease as described (23). The cleaved FXYD1 was then added to the solubilized yeast membranes with the Na,K-ATPase bound to BD-Talon beads at a molar ratio of 10:1 (FXYD1/Na,K-ATPase) and incubated overnight. After washing off the excess FXYD1, the $\alpha\beta$FXYD1 complex was eluted as usual.

Na,K-ATPase Activity Measurements—Enzyme activity was measured using the PiColor Lock malachite green assay (Innova Biosciences) detecting free phosphate from ATP hydrolysis in a medium containing 130 mM NaCl, 20 mM KCl, 3 mM $MgCl_2$, 1 mM EGTA, 25 mM histidine, pH 7.4, and 1 mM ATP at 37 °C. For ion titrations, activity was measured at varying concentrations of Na^+ plus choline chloride and KCl (80 mM) with constant total ionic strength (170 mM total).

Data were fitted using KaleidaGraph (Synergy Software). Na^+ ion titrations were fitted using the Hill equation.

$$V([Na^+]) = V_{max} \cdot \frac{[Na^+]^{n_H}}{(K_{0.5}Na)^{n_H} + [Na^+]^{n_H}} \quad \text{(Eq. 1)}$$

Determination of Phosphoenzyme—Phosphoenzyme was determined as described previously (29).

Preparation of Proteoliposomes—Proteoliposomes were prepared with lipid mixtures of synthesized lipids. The composition of 34 mol % DPPC and 10 mol % cholesterol was kept constant, whereas DOPS was varied between 0 and 30 mol %, and DOPE was varied between 56 and 26 mol % to complement all compounds to 100 mol %. Due to the lower solubility of such lipid mixtures in DDM only, a solution of 1% DDM and 1% $C_{12}E_8$ in Buffer H (25 mM imidazole, 1 mM EDTA, 5 mM $MgSO_4$, 5 mM Na_2SO_4, 70 mM K_2SO_4, pH 7.2) was chosen to solubilize the lipids. Proteoliposome formation containing recombinant α1His_{10}-β1FXYD1 complexes was performed as described previously (24). In short, to obtain a lipid concentration of 8 mg/ml, the desired lipid mixture was dissolved in Buffer H with 2% DDM. Sulfate was chosen as primary anion because it produces a significantly lower leak current than chloride (26). The purified recombinant enzyme complexes were diluted with Buffer H to obtain a protein concentration of 0.1 mg/ml and mixed with the lipid/DDM mixture at a ratio of 1:1 (v/v). Bio beads (1 mg of beads per 2 μl of lipid/DDM mixture) were added, and the mixture was incubated overnight at 6 °C under continuous stirring. The solution containing the vesicles was separated from the sedimented beads using capillary tips and stored at 0 °C. After a minimum of 3 h on ice, tight vesicles were ready for further use. Besides recombinant α1His_{10}-β1 complexes with FXYD1 as control, preparations were assembled with enzyme complexes containing phosphorylated FXYD1-P (at Ser-68) or the S63E, S68E, and S63E,S68E mutants.

Fluorescence Experiments with Oxonol VI—The negatively charged fluorescent dye oxonol VI has been introduced previously as an indicator of inside-positive membrane potentials in vesicles (26), and it has been shown to detect successfully the electrogenic pump activity of the α1His_{10}-β1 reconstituted in proteoliposomes. Experiments were performed corresponding to a recent study from this laboratory (24). In short, 1 ml of buffer solutions containing 25 mM imidazole, 1 mM EDTA, 2.5 mM $MgSO_4$, and various concentrations of Na_2SO_4, pH 7.2, were thermally equilibrated in a cuvette equipped with a magnetic stirrer. Afterward, 25 nM oxonol VI and a volume of proteoliposomes corresponding to 80 μg/ml lipid were added. When a steady-state fluorescence level was obtained, 2.5 mM MgATP was added to trigger pump activity. The pump activity is reflected in a fluorescence increase that exponentially approaches a steady-state level at which the pump current is compensated by the leak current due to the membrane conductance. The experiments were carried out in a PerkinElmer Life Sciences LS 50B luminescence spectrometer. The excitation wavelength was set to 580 nm (slit width 15 nm), and the emission wavelength was set to 660 nm (slit width 15 nm). Measurements were performed at 20 °C. To allow a comparison between different experiments, the fluorescence changes were normalized with respect to the fluorescence level at membrane voltage 0 (F_0) before the addition of ATP. The normalized fluorescence increase was fitted with a single exponential function,

$$F_{norm}(t) = \frac{F(t) - F_0}{F_0} \cdot (1 - e^{-t/\tau}) \quad \text{(Eq. 2)}$$

where $F_{norm}(t)$ is the normalized fluorescence amplitude, $F(t)$ is the measured fluorescence, and τ is a characteristic time constant that reflects the pump activity. The initial slope of the fluorescence increase after ATP addition, $dF_{norm}(t)/dt$, corresponding to the increase in membrane potential, is proportional to the product of the pumping rate and the amount of active pump molecules, averaged over all vesicles in the solution (26). The initial slope was determined as described recently (24) and used as parameter to determine the pump rate. Its dependence on the extravesicular Na^+ concentration has to be determined for each series with the same vesicle preparation and can be exploited to evaluate the $K_{0.5}{}^{Na}$ of Na^+ ions for activation of the ion pump (26).

Stopped-Flow Experiments with RH421—Stopped-flow measurements (27) were performed with an Applied Photophysics SX20 system. To detect electrogenic reaction steps with RH421, the monochromator for excitation was set to 577 ± 6 nm. The emitted light was collected at wavelengths of ≥665 nm using a cut-off filter. Measurements were carried out at 23 or 30 °C, and the solutions were mixed in a ratio of 1:1 using 120 μl/syringe.

For the reaction $3NaE_1 + ATP \rightarrow E_2P + 3Na^+$, syringe 1 was loaded with 10 μg/ml purified Na,K-ATPase, 300 nM RH421, 100 mM NaCl, and 4 mM $MgCl_2$. Syringe 2 contained 100 mM NaCl, 4 mM $MgCl_2$, and 1 mM ATP.

For the reaction $E_2(2K) + 3Na^+ + ATP \rightarrow 3NaE_1ATP + 2K^+$, syringe 1 was filled with 30 μg/ml Na,K-ATPase, 300 nM RH421, 20 mM KCl (or RbCl), 1 mM EDTA, and syringe 2 was filled with 100 mM NaCl, 1 mM EDTA, and 2 mM ATP (0 Mg^{2+}).

All solutions were buffered at pH 7.2 using MOPS/Tris. Choline chloride was added appropriately to the buffer solutions to keep the ionic strength constant at 120 mM. The fluorescence signals were detected for up to t_{max} = 500 ms. To compare various experiments, the fluorescence amplitude was normalized according to Equation 3,

$$F_{norm}(t) = \frac{F(t)}{F(t_{max}) - F(t_0)} \quad \text{(Eq. 3)}$$

where $F(t_0)$ is the fluorescence level at $t = 0$, the time point when the detection chamber is filled with the reaction mixture, and $F(t_{max})$ is the level after 500 ms. Traces from 15 individual shots were averaged.

Data were fitted using KaleidaGraph (Synergy Software). Stopped-flow traces were fitted to a monoexponential function,

$$F = A \cdot e^{-k \cdot t} + c \quad \text{(Eq. 4)}$$

or double exponential function,

$$F = A_1 \cdot e^{-k_1 \cdot t} + A_2 \cdot e^{-k_2 \cdot t} + c \quad \text{(Eq. 5)}$$

where A is the amplitude of the fluorescence signal, k is the rate of the reaction, and c is the equilibrium fluorescence level after the reaction is complete.

Computational Docking—Computational docking was used to determine a plausible location for the C-terminal helix (residues 60–70) of FXYD1. The NMR structure of free FXYD1 (Protein Data Bank code 2jo1) provides a range of conformers for this segment (10). Each of them was docked to the E_2 conformation of the Na,K-ATPase) in an occluded state with two rubidium ions bound (as potassium congeners (Protein Data Bank code 3kdp) (11) using the geometric-electrostatic-hydrophobic (GEH) version of MolFit (33–35). Arginine residues Arg-71 and Arg-72, which show high backbone mobility in the NMR study, were not included in the docking computations. MolFit performs a stepwise scan in six dimensions. One molecule, usually the larger one, is kept fixed, and the other is rotated and translated in steps, and a GEH complementarity score is calculated for each step; higher scores indicate better complementarity. Although the α subunit and FXYD1 are treated as rigid bodies, MolFit allows for small conformational adjustments, which may occur upon complex formation, by softening the molecular surface and absorbing limited clashing. In addition, the flexible side chains of exposed lysine residues are trimmed to reduce possible clashes, but their electrostatic effect is maintained (36). The GEH scores have arbitrary units and depend on the scanning parameters. Therefore, standard scan intervals of 12° and 1.05 Å were used in all of the scans. Statistical analysis of the docking scores was executed by fitting an extreme value distribution function to the distribution of scores (37). The fit provided estimates of the mean score, μ = 525, and the S.D., σ = 90. The GEH scan is followed with a post-scan filtering step in which the predicted interfaces are reevaluated using additional measures: the desolvation energy, the statistical preference of residues to be present in the interface, and pairwise contact preferences (38). Two additional tests were executed on the docking models, requesting that the termini of the docked segment 60–70 of FXYD1 be exposed in the predicted complex and that the N-terminal end of the docked segment (residue 60) be at a reasonable distance from the C-terminal end of the N-terminal helix of FXYD1 (residue 49). UCSF Chimera was used for structure superposition and visualization of the docking results and to prepare the figures (39).

The models from the 20 docking searches, one for each NMR conformer of FXYD1 segment 60–70 (10), were combined and clustered. They produced four clusters, three of which localize segment 60–70 in the elongated groove between the intracellular Na,K-ATPase domains N and P, and a fourth, with significantly lower GEH scores, that binds in an elongated depression on the surface of the transmembrane helices. Docking models from the first three clusters were refined in two steps: (*a*) local rigid body refinement with MolFit in which small angular rotations in steps of 2° were used to obtain the highest GEH score and (*b*) energy minimization of the complex, keeping the Cα atoms of Na,K-ATPase restrained to their starting positions and allowing the side chains and the docked FXYD1 segment to adjust. Minimization was performed with Discovery Studio (Discovery Studio Modeling Environment, Accelrys Software, Inc., San Diego, CA). To establish independently the validity of the docking model, we determined the preferred binding locations of single amino acids on the surface of Na,K-ATPase using ANCHORSmap (40). ANCHORSmap scatters numerous amino acid probes on the surface of a protein and detects low ΔG binding locations (anchoring spots) taking into consideration that the excised amino acid is part of an approaching hypothetical protein. Anchoring spots with $\Delta G < -4$ kcal/mol were found to correspond to experimentally determined hot spot residues.

Results

Fig. 1 shows an SDS-polyacrylamide gel of the high specific activity purified human $\alpha1\beta1$ and reconstituted $\alpha1\beta1$FXYD1 complexes prepared by the gravity column procedure (see "Methods"). The Coomassie Blue-stained gel illustrates the high purity of the preparation in which only the α and β subunits (with two glycosylated forms), without or with the reconstituted FXYD1 protein, are present in significant amounts. The BD-Talon beads were washed, and the protein was eluted in a medium containing 0.12 mg/ml C12E8, 0.07 mg/ml SOPS, 0.07 mg/ml SOPC, and 0.025 mg/ml cholesterol (see "Methods"). The rather high concentration of phospholipids used to make the preparations is important to maintain full stability of the control sample, which is inherently less stable than those made with FXYD1 (22, 23). This feature allows assessment of the true kinetic effects of the FXYD1 protein without the contribution of superimposed stabilizing effects of FXYD1,

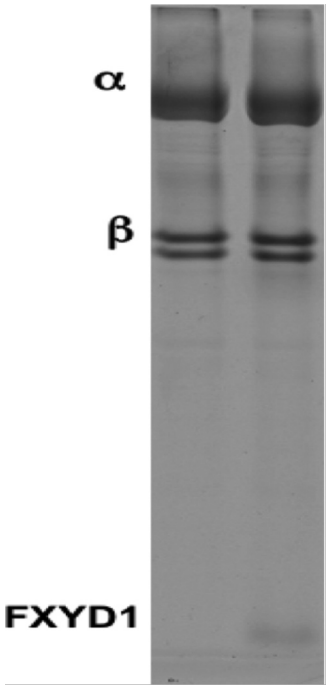

FIGURE 1. **Purified Na,K-ATPase: $\alpha1\beta1$ and $\alpha1\beta1$FXYD1.** 10 μg of column-purified $\alpha1\beta1$ or $\alpha1\beta1$FXYD1 complexes of high Na,K-ATPase specific activity (see Table 3) were applied to each lane.

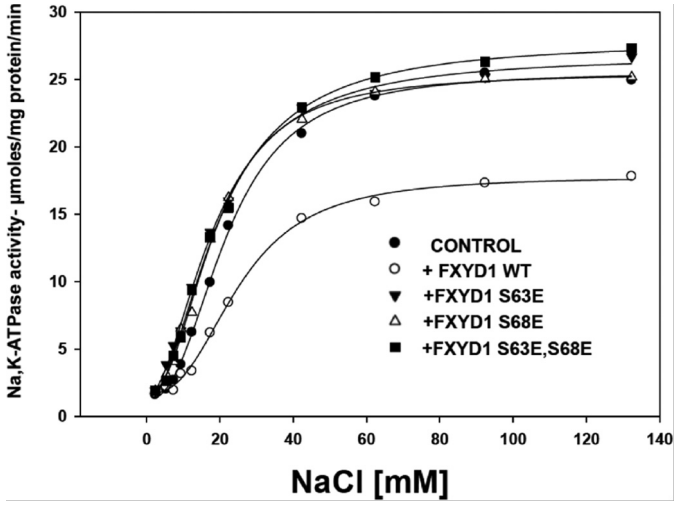

FIGURE 2. **Effects of wild-type FXYD1 and phosphomimetic mutants on Na,K-ATPase activity of $\alpha1\beta1$ at varying Na^+ concentrations.** Experimental points and best fit curves are presented for Control ($\alpha1\beta1$), +WT FXYD1, +FXYD1 S68E, +FXYD1S63E, and +FXYD1S63E,S68E. Experimental points were carried out in triplicate, but for clarity, error bars, all with amplitudes ≤10% of the values, have been omitted.

observed previously as an apparent increase in V_{max} compared with the partially inactivated control (41).

Effects of FXYD1 and Phosphomimetic Mutants on Na,K-ATPase Activity—The Na,K-ATPase activity of the purified detergent-solubilized protein ($\alpha1\beta1$) was measured as a function of the Na^+ concentration in the incubation medium. Fig. 2 shows Na^+ activation curves for Na,K-ATPase activity of the control and of the four tested complexes of $\alpha1\beta1$ with WT FXYD1 or the FXYD1S63E, FXYD1S68E, or FXYD1S63E,S68E mutant, respectively. The concentration dependence has been fitted with the Hill function, shown under "Methods."

Table 2 summarizes the kinetic parameters (V_{max}, $K_{0.5}$Na, and n_H) of the best fit curves for two full experiments in all five conditions, using different enzyme preparations. Measurements with and without FXYD1 were performed 5–7 times with average $K_{0.5}$Na values as follows: control, 22.5 ± 0.48 mM ($n = 5$); with FXYD1, 24.83 ± 0.62 mM ($n = 7$); and with phosphomimetic mutants, 18.21 ± 0.35 mM ($n = 6$). The last two columns of the table depict the average values for all of the experiments. The obvious effects of WT FXYD1 are a 25–30% inhibition of V_{max} and an increase of $K_{0.5}$Na on the order of 15–20%, with no systematic effect on n_H. By contrast, all three phosphomimetic mutants abolish the effect of FXYD1 on V_{max} and reduce $K_{0.5}$Na to values below that of the control. The differences of $K_{0.5}$Na between control and +FXYD1 ($p < 0.01$) and between phosphomimetic mutants and both wild-type FXYD1 and control ($p \leq 0.0001$) are all significant. The maximal turnover rates with and without FXYD1 (Table 3) were estimated by comparing the Na,K-ATPase activity (V_{max}) of complexes at saturating Na^+ and K^+ concentrations (140 mM Na^+ and 20 mM K^+), and the active-site concentration was estimated from the phosphoenzyme level (4.2–4.3 nmol/mg protein). From these measurements (7–9 experiments), it is seen that FXYD1 reduced the maximal turnover rate by about 25%, from 8163 ± 284 to 6248 ± 115 min^{-1} ($p < 0.0001$). The combined effects of FXYD1, to reduce turnover rate and increase $K_{0.5}$Na, lead to a significant overall reduction of Na,K-ATPase activity, particularly at subsaturating Na^+ concentrations, similar to those in physiological conditions. For example, at a cytoplasmic concentration of 15 mM Na^+ (and 80 mM K^+), using the average best fit parameters derived for all experiments (see Table 2) and the Hill function above, the ratio of Na,K-ATPase activities for $\alpha1\beta1$FXYD1/$\alpha1\beta1$ is calculated to be close to 0.65, namely inhibition of about 35% by FXYD1. Conversely, the strongly reduced $K_{0.5}$Na for the phosphomimetic mutants leads to a ratio of rates of Na,K-ATPase activity for $\alpha1\beta1$FXYD1S68E/$\alpha1\beta1$FXYD1 of 1.95, namely a 95% increase in rate for the phosphomimetic mutant compared with the FXYD1.[4] The experiments in Fig. 2 and Tables 2 and 3 (also see Table 5) were performed with proteins prepared in elution buffers containing both SOPS and SOPC, but essentially the same inhibitory effects of FXYD1 were observed when only SOPS was used to prepare the protein. For example, in another series of comparative experiments, the ratios of the maximal Na,K-ATPase activity $\alpha1\beta1$FXYD1/$\alpha1\beta1$ were 0.73 ± 0.040 ($n = 7$) for preparations made with SOPS/SOPC/cholesterol or 0.672 ± 0.04 ($n = 5$) for preparations made with SOPS/cholesterol.

The Na,K-ATPase activity of the $\alpha2\beta1$ isoform without and with FXYD1 has also been measured as function of the Na^+ concentration. Table 4 contains the corresponding fitted parameters. The effects of FXYD1 on $\alpha2\beta1$ were significant and similar to those of $\alpha1\beta1$ but were more modest in magnitude;

[4] In a real physiological situation associated with the phosphorylated FXYD1, the increase in rate of pumping would be greater than the 95% calculated here because the cytoplasmic Na^+ concentration would itself be raised compared with the assumed resting concentration of 15 mM.

TABLE 2

Effects of FXYD1 and phosphomimetic mutants on V_{max} and $K_{0.5}$ Na for activation of Na,K-ATPase activity ($\alpha1\beta1$)

The values in columns 2–5 represent best fit parameters ± S.E. for two experiments using two different enzyme preparations not reconstituted (control) or reconstituted with WT FXYD1, FXYD1S63E, FXYD1S68E, or FXYD1S63E,S68E. The average values of $V_{max}(\alpha1\beta1FXYD1)/ V_{max}(\alpha\beta)$, $K_{0.5}$Na ± S.E., and n_H ± S.E. (columns 6 and 7) are quoted for all experiments done in the same conditions as the two full experiments (*i.e.* seven experiments for control without or without WT FXYD1). The average values of $K_{0.5}$Na and n_H for all three mutants (*i.e.* data from six experiments) were calculated on the assumption there are no significant differences between the mutants. The *p* values in the $K_{0.5}$Na column are for control compared with WT FXYD1 (line 3) and control compared with mutants or FXYD1 compared with the mutants (line 5). Expt., experiment.

	Expt. 1 V_{max}	$K_{0.5}$Na, n_H	Expt. 2 V_{max}	$K_{0.5}$Na, n_H	Average V_{max} ($\alpha1\beta1$FXYD1)/V_{max}($\alpha\beta$)	Average $K_{0.5}$Na, n_H
	μmol/min/mg	*mM*	*μmol/min/mg*	*mM*		*mM*
$\alpha1\beta1$	25.5 ± 1.76	21.71 ± 1.61, 1.6 ± 0.2	17.85 ± 1.58	20.74 ± 1.2, 2.33 ± 0.24		22.5 ± 0.5, 2.25 ± 0.14 ($n = 5$)
$\alpha1\beta1$FXYD1 WT	17.1 ± 0.85	25.25 ± 0.88, 2.55 ± 0.2	15.35 ± 0.45	25.35 ± 2.4, 1.77 ± 0.2	0.73 ± 0.040 ($n = 7$)	24.83 ± 0.6, 2.19 ± 0.12 ($n = 7$) ($p < 0.02$)
$\alpha1\beta1$FXYD1S63E	27.6 ± 0.93	18.36 ± 0.45, 2.01 ± 0.1	17.14 ± 0.57	17.68 ± 0.68, 1.75 ± 0.1	1.03 ($n = 2$)	
$\alpha1\beta1$FXYD1S68E	27.4 ± 1.07	18.93 ± 0.53, 2.05 ± 0.12	18.8 ± 0.63	17.64 ± 0.7, 1.93 ± 0.1	1.06 ($n = 2$)	18.21 ± 0.35, 2.01 ± 0.12 ($n = 6$) ($p \leq 0.0001$)
$\alpha1\beta1$FXYD1S63E, S68E	29.07 ± 1.03	19.45 ± 0.59, 1.9 ± 0.11	22.6 ± 0.75	17.21 ± 0.54, 1.93 ± 0.1	1.2	

TABLE 3

Effect of FXYD1 on Na,K-ATPase ($\alpha1\beta1$) turnover rate at 37 °C

Note that the enzyme was prepared with both SOPS and soy phosphatidylcholine (see "Methods") and has a specific activity similar to that of purified pig kidney enzyme (58).

	Na,K-ATPase activity	EP	Turnover rate	Ratio of turnover rates ± S.E. ($\alpha1\beta1$FXYD1/$\alpha1\beta1$)
	μmol/min/mg protein	*nmol/mg protein*	*min−1*	
$\alpha1\beta1$	37.2 ± 2.3 ($n = 9$)	4.42 ± 0.23 ($n = 9$)	8163 ± 284	
$\alpha1\beta1$FXYD1	27.2 ± 1.0 ($n = 7$) ($p < 0.0001$)	4.31 ± 0.15 ($n = 7$)	6248 ± 115 ($n = 7$) ($p < 0.0001$)	0.76 ± 0.03

TABLE 4

Effects of FXYD1 on V_{max} and $K_{0.5}$Na for $\alpha2\beta1$

	Na,K-ATPase activity	$K_{0.5}$Na
	μmol/mg/min	*mM*
Without FXYD1	20.2 ± 0.5	17.65 ± 0.45
With FXYD1	17.3 ± 0.4 ($n = 4$, $p = 0.0044$)	20.11 ± 0.71 ($n = 4$, $p = 0.028$)

namely, FXYD1 reduced V_{max} by about 15% and increased $K_{0.5}$Na by about 12%. We have also measured the K_i for vanadate inhibition of the $\alpha2\beta1$ Na,K-ATPase in the absence and presence of FXYD1. The K_i values were 6.3 ± 0.15 μM (−FXYD1, $n = 8$) and 3.32 ± 0.3 μM (+FXYD1, $n = 8$), respectively.

The abolishment of the kinetic effects of wild-type FXYD1 by the S63E, S68E, and S63E,S68E mutants, seen in Fig. 2 and Table 2, suggests that the mutations altered the interaction of the cytoplasmic helix H4 with the α subunit and raise the issue of whether the mutated proteins are still associated with the α subunit or, perhaps, are completely dissociated. An answer to this question was obtained in experiments to assess stabilization of the Na,K-ATPase activity by both wild-type and mutated FXYD1 (Fig. 3). As described previously, all FXYD proteins, but especially FXYD1, protect the Na,K-ATPase activity against either thermal or detergent-mediated inactivation by a mechanism involving amplification of the phosphatidylserine binding to the protein (23). The control enzyme $\alpha1\beta1$ and the reconstituted $\alpha1\beta1$FXYD1 complexes, wild type or the different phosphomimetic mutants, were heated to 45 °C for 30 min before the Na,K-ATPase activity was measured. In the control, Na,K-ATPase activity was reduced to about 35% of the initial activity, whereas all reconstituted complexes ($\alpha1\beta1$FXYD1, $\alpha1\beta1$FXYD1S63E, $\alpha1\beta1$FXYD1S68E, and $\alpha1\beta1$FXYD1S63E,S68E) were strongly protected, the activity being maintained at about 80% of the initial value. The persistence of the stabilizing effect for the phosphomimetic mutants is consistent with a previous observation that stabilization by FXYD1 is not abolished by phosphorylation of the FXYD1 at Ser-68. In short, both wild type and phosphomimetic mutants must still be associated with the $\alpha1\beta1$ complex, presumably via the transmembrane segment, whereas the interactions of the cytoplasmic helix are different, as will be discussed below.

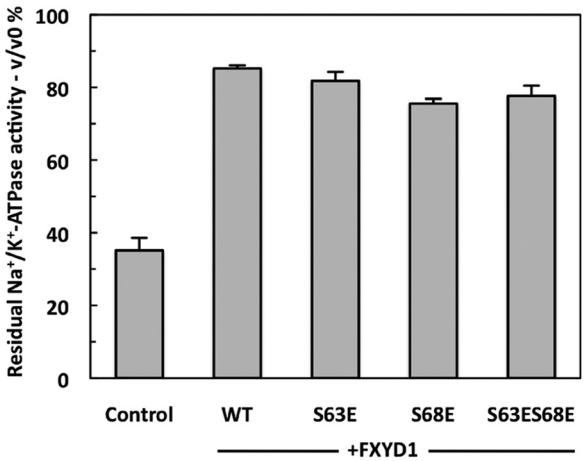

FIGURE 3. **Stabilization of Na,K-ATPase ($\alpha1\beta1$) by wild-type FXYD1 and phosphomimetic mutants.** Control ($\alpha1\beta1$), +WT FXYD1, +FXYD1 S68E, +FXYD1S63E, and +FXYD1S63E,S68E complexes were heated to 45 °C for 30 min. Na,K-ATPase activity was then measured in triplicate. Results are presented as a percentage of control prior to heating (v/v_0) ± S.E. (*error bars*).

Mechanism of Kinetic Effects of FXYD1—The effects of wild-type FXYD1 and the phosphomimetic mutants on the steady-state kinetic properties of the Na,K-ATPase beg the question of their detailed mechanism. In principle, the FXYD1-mediated inhibition of the steady-state V_{max} and rise in $K_{0.5}$Na for Na,K-ATPase activity (as well as reduced K_i for inhibition by vanadate) could all be indicative of a partial stabilization of the E_2(2K) conformation. A reduction of the maximal turnover rate by FXYD1 is

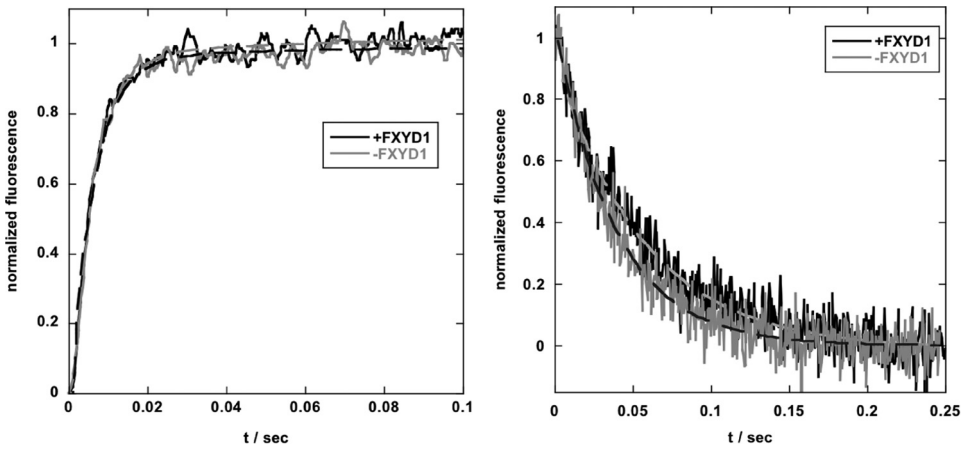

FIGURE 4. **Stopped-flow traces of conformational changes for $\alpha 1\beta 1$ without and with FXYD1.** *Left*, $E_1P(3Na) \rightarrow E_2P$; *right*, $E_2(2K)ATP \rightarrow E_1 3NaATP$. Each trace represents the average of 15 separate shots. *Gray*, control; *black*, +FXYD1.

necessarily caused by a partial inhibition of rate-limiting steps of the enzymatic cycle, namely either or both of the conformational changes, $E_1P(3Na) \rightarrow E_2P$ and $E_2(2K)ATP \rightarrow E_1 3NaATP$.

We have addressed this question directly using the electrochromic dye RH421 and the stopped-flow technique. These experiments permit determination of rate constants of the rate-limiting partial reactions. The RH421 fluorescence detects changes in the local electric field associated with electrogenic ion-binding and dissociation reactions. These effects were first described in detail using the purified renal Na,K-ATPase embedded in membrane fragments and, as shown more recently, also in the purified detergent-solubilized renal and recombinant Na,K-ATPase (25, 42, 43). Standard RH421 fluorescence changes detect ion binding and dissociation in three partial reactions of the pump cycle: (*a*) Na^+ binding in the E_1 conformation, $E_1 + 3\ Na^+ \rightarrow 3NaE_1$; (*b*) ATP/Mg-induced transition from E_1 in the presence of Na^+ to E_2P and Na^+ release ($3NaE_1 \rightarrow E_2P + 3Na^+$); and (*c*) K^+ binding to the E_2 conformation ($E_2P + 2K^+ \rightarrow E_2(2K)$). Equilibrium Na^+ and K^+ titrations of RH421 fluorescence signals (*a* and *c*) provide a measure of the intrinsic binding affinities of $3Na^+$ ions to E_1 and of $2K^+$ ions to E_2P, respectively. Previously, we have reported that FXYD1 binding to $\alpha 1\beta 1$ induces a rise in the intrinsic binding affinity of Na^+ but not of K^+ (or Rb^+) (43). In stopped-flow experiments, the protein undergoes the $3NaE_1 \rightarrow E_2P$ reaction when the Na,K-ATPase, prebound with Na^+ and Mg^{2+}, is mixed with ATP. Similarly, the protein undergoes the $E_2(2K/Rb)ATP \rightarrow 3NaE_1ATP$ transition when the enzyme, prebound with K^+ or Rb^+ ions, is mixed with Na^+ plus ATP. The time course of the interconversion between the initial and final charged states does not track cation binding or release directly because cation binding and release are diffusion-controlled processes and are orders of magnitude faster than the preceding conformation transition. Rather, the time course tracks the rate-limiting conformational transitions, namely $3NaE_1P \rightarrow E_2P3Na$ in the ATP-induced reaction or $E_2(2K)ATP \rightarrow E_1(3Na)ATP$, respectively. A recent example of measurements of the rates of the conformational changes using the purified human $\alpha 1\beta 1$FXYD1 complex can be seen in Ref. 27. Fig. 4 shows the time course of fluorescence traces corresponding to $3NaE_1P \rightarrow E_2P$ (*left*) and $E_2(2Rb)ATP \rightarrow 3NaE_1ATP$ (*right*) for the $\alpha_1\beta_1$ isoform, with and without FXYD1. In Table 5, the fitted rate constants of the conformation transitions are compiled for both types of reaction. The fluorescence signals of the reaction $3NaE_1P \rightarrow E_2P$ are fitted with a sum of two exponentials, a behavior that was observed also in the case of native Na,K-ATPase isolated from shark salt gland (44). However, the minor slow process contributed less than 10% to the total fluorescence increase. For the dominant fast process with a rate of 170 s^{-1}, no difference was found without or with FXYD1. For the second type of experiment that detects $E_2(2K/2Rb)ATP \rightarrow 3NaE_1ATP$, the presence of FXYD1 reduced the rate constant by 28–36% when measured at either 23 or 30 °C. Fig. 5 and Table 6 show the corresponding results of experiments with the $\alpha 2\beta 1$ isoform with and without FXYD1. As in the case of the $\alpha 1\beta 1$ complex, FXYD1 has no effect on the $3NaE_1P \rightarrow E_2P$ reaction (*left*) but reduces the rate of the Rb^+ (or K^+)-dependent transition, $E_2(2Rb)ATP \rightarrow 3NaE_1ATP$, by about 25% (*right*). The difference between the traces of $E_2(2Rb)ATP \rightarrow 3NaE_1ATP$ transition appears a bit more distinct for the $\alpha 2\beta 1$ complex than for the $\alpha 1\beta 1$ complex. This is due to the lower rates and better signal/background ratio, but the effects are quite reproducible and significant for both isoform complexes.

A final point concerns a lack of effect of FXYD1 when the conformation transition back to E_1 is performed in the absence of ATP, $E_2(2Rb) \rightarrow 3NaE_1$ (Table 5, bottom line). To induce this reaction, syringe 1 was filled with 30 μg/ml Na,K-ATPase, 300 nM RH421, 20 mM KCl (or RbCl), 1 mM EDTA, and syringe 2 was filled with 100 mM NaCl and 1 mM EDTA only. In the absence of ATP, only a slow rate on the order of 0.37 s^{-1} was observed for the reaction $E_2(2K) \rightarrow E_1 3Na$ in the presence and absence of FXYD1. A similarly slow transition has been observed previously using FITC-labeled Na,K-ATPase from pig kidney (45). In contrast to the non-covalently bound probe RH421 used here, the pig kidney protein was labeled with FITC selectively at Lys-515 and is therefore unable to bind ATP, thus precluding measurement of the conformational transition with ATP bound to the low affinity binding site. The different effect of FXYD1 on the rate-limiting reaction step in the absence and presence of ATP indicates that different molecular processes control the conformational transition in both conditions, so that the reaction rate, in the absence of ATP, is controlled by an

TABLE 5

Rates of conformational changes for $\alpha 1\beta 1$ without and with FXYD1

Individual values of the rates represent the average of 15 shots. Values in the table are expressed as averages ± S.E. for $n \geq 3$ or averages for $n = 2$.

	T	−FXYD1	+FXYD1	+FXYD1/−FXYD1
	°C	s^{-1}	s^{-1}	
$3NaE_1 + ATP \rightarrow E_2P$	23	$k_1 = 170 \pm 8.0$, $k_2 = 30 \pm 3.8$ ($n = 3$)	$k_1 = 170 \pm 6.5$, $k_2 = 21 \pm 2.3$ ($n = 3$)	1.0
$E_2(2Rb) + ATP \rightarrow E_1 3NaATP$	23	24.3 ± 2.19 ($n = 4$)	15.5 ± 1.18 ($n = 4$) ($p = 0.01$)	0.64
$E_2(2Rb) + ATP \rightarrow E_1 3NaATP$	30	45 (average of 2)	32 (average of 2)	0.71
$E_2(2K) + ATP \rightarrow E_1 3NaATP$	30	80 (average of 2)	58 (average of 2)	0.725
$E_2(2Rb) \rightarrow E_1 3Na$	23	0.37 (average of 2)	0.36 (average of 2)	0.97

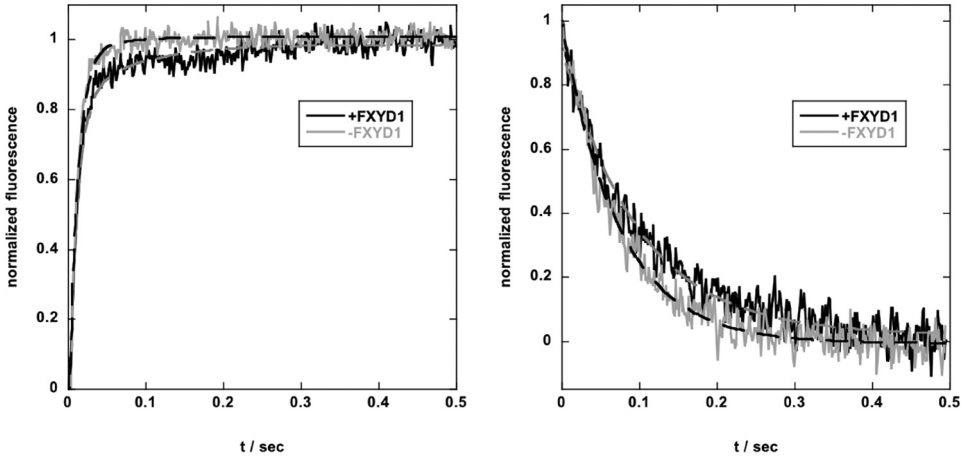

FIGURE 5. **Stopped-flow traces of conformational changes for $\alpha 2\beta 1$ without and with FXYD1.** *Left*, $E_1P(3Na) \rightarrow E_2P$; *right*, $E_2(2K)ATP \rightarrow E_1 3NaATP$. Each trace represents the average of 15 separate shots. *Gray*, control; *black*, +FXYD1.

TABLE 6

Rates of conformational changes for $\alpha 2\beta 1$ without and with FXYD1 at 23 °C

Individual values of the rates represent the average of 15 shots. Values in the table are expressed as averages for two experiments.

	−FXYD1	+FXYD1	Ratio +FXYD1/−FXYD1
	s^{-1}	s^{-1}	
$3NaE_1 + ATP \rightarrow E_2P$	$k_1 = 90.6$, $k_2 = 18.5$	$k_1 = 91.3$, $k_2 = 13$	0.99
$E_2(2Rb) + ATP \rightarrow E_1 3NaATP$	13.7	10.2	0.74

extremely slow process that is unaffected by the presence of FXYD1.

Effects of FXYD1 and Phosphomimetic Mutants on the Na,K-ATPase Reconstituted in Proteoliposomes—We have shown recently that after reconstitution of the detergent-soluble recombinant Na,K-ATPase into proteoliposomes, generation of the pump-mediated electrogenic potential is conveniently detected using the voltage-sensitive dye, oxonol VI (24). These experiments allow determination of the half-saturating Na^+ concentration, $K_{0.5}$Na for generation of the electrogenic potential accompanying Na,K-ATPase activity with and without FXYD and the three phosphomimetic mutants. The recent experiments have shown that FXYD1 significantly raises $K_{0.5}$Na in proteoliposomes made only with phosphatidylcholine, but either phosphorylation of FXYD1 on Ser-68 or inclusion of even small amounts of excess DOPS (≥5 mol %) into the proteoliposomes abrogates the effect.[5] Therefore, we have now reconstituted proteoliposomes with all five recombinant complexes, $\alpha 1His_{10}$-$\beta 1$, $\alpha 1His_{10}$-$\beta 1$FXYD1, $\alpha 1His_{10}$-$\beta 1$FXYD1S68E, $\alpha 1His_{10}$-$\beta 1$FXYD1S63E, and $\alpha 1His_{10}$-$\beta 1$FXYD1S63E,S68E, and phospholipid compositions with 0, 5, 10, 18, and 30 mol % DOPS. At least two different enzyme preparations were used for each type of WT FXYD1 or S63E, S68E, and S63E,S68E mutant proteins. With each vesicle preparation, the initial slope of the ATP-dependent oxonol VI fluorescence signal was measured (in triplicate) in buffers containing nine Na^+ concentrations between 0 and 50 mM. Because the initial slope of the oxonol VI fluorescence signal is proportional to the rate of active pumping and the number of active ion pumps per vesicle is constant within the same proteoliposome preparation, the initial slopes in the same preparation can be compared directly and plotted against the respective Na^+ concentration (24). The concentration dependence was fitted by the Hill function to obtain the half-saturating Na^+ concentration, $K_{0.5}$Na, for generation of the electrogenic potential. The results in Fig. 6 show the effects of the wild-type FXYD1 and the phosphomimetic mutants as well as the data on phosphorylated FXYD1 (Ser-68) taken from Ref. 24. Consistent with our recent report, the wild-type FXYD1 significantly raised the $K_{0.5}$Na in proteoliposomes made only with phophatidylcholine, compared with the control without FXYD1, and in proteoliposomes made with added DOPS (≥10% mol %) the effect was abolished. All three phos-

[5] Note that all purified Na,K-ATPase preparations are eluted from BD-Talon beads in a solution containing SOPS, which is absolutely required for stability. Thus, abrogation of the effect of FXYD1 in the proteoliposomes reflects the effect of excess DOPS.

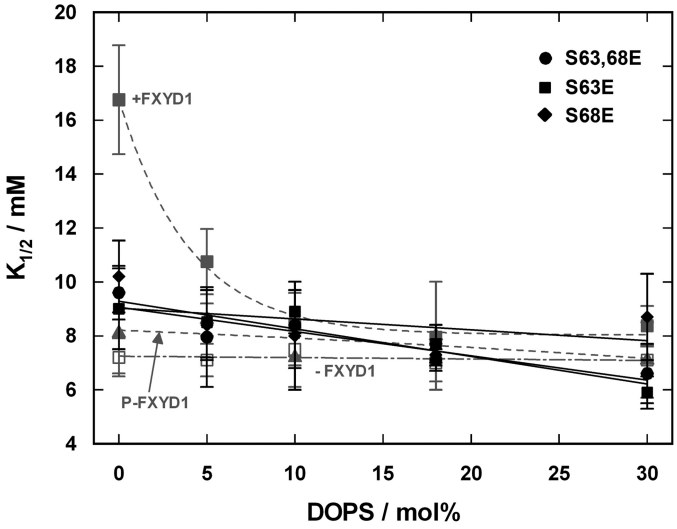

FIGURE 6. **Effects of wild-type FXYD1 and phosphomimetic mutants on $K_{0.5}$Na in proteoliposomes prepared with increasing mole fractions of DOPS.** α_1His$_{10}$-β_1 complexes with three mutant FXYD1 subunits, S63E (*solid squares*), S68E (*solid diamonds*), and S63E,S68E (*solid circles*), were prepared in lipid mixtures containing 10 mol % cholesterol, 34 mol % DPPC, and 56 mol % (DOPS + DOPE). $K_{0.5}$Na for generation of the electrogenic voltage is plotted as a function of the fraction of DOPS in the membranes. The results obtained with native FXYD1 (24) and phosphorylated FXYD1 (*P-FXYD1*) are included as *gray squares* and *triangles*, respectively. The *straight lines* are linear regression curves. The *line* through the native FXYD1 data is drawn to guide the eye. *Error bars*, S.E.

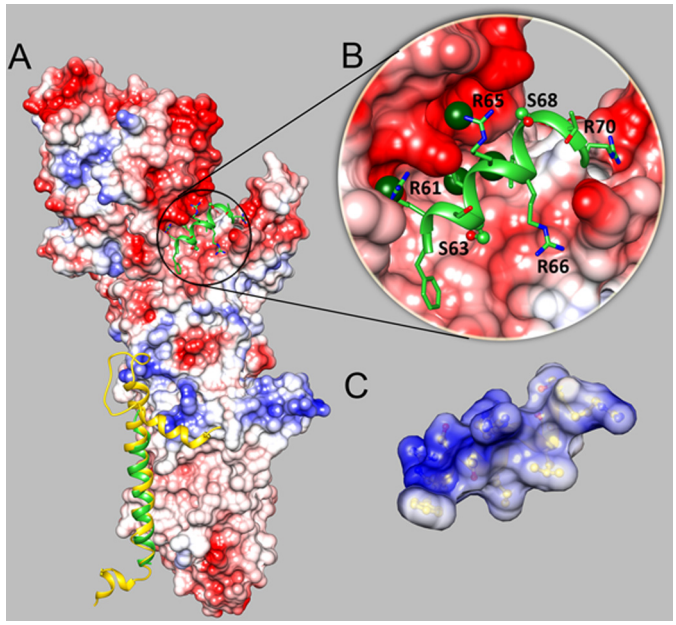

FIGURE 7. **Computational model of the binding of the cytoplasmic H4 helix of FXYD1 to the E_2 conformation of the Na,K-ATPase.** The E_2 conformation of the Na,K-ATPase (Protein Data Bank code 3kdp) was used for the modeling. The electrostatic potential of the surface of the α-subunit is *colored white* for neutral, *red* for negative, and *blue* for positive potentials. *A*, superposition of the transmembrane helix of free FXYD1 (*yellow*) (10) onto the transmembrane helix of FXYD2 (*green*) and the predicted location of segment 60–70 (*green* with side chains shown). *B*, *enlargement* of the predicted binding state of FXYD1. The four arginine residues, Arg-61, Arg-65, Arg-66, and Arg-70, point toward negative surface regions of Na,K-ATPase, and the hydrophobic residues Phe-60, Ile-64, and Leu-67 point toward the hydrophobic region at the bottom of the trough between the P and N domains. Residues Ser-63 and Ser-68, shown as *ball-and-stick representations*, point toward negatively charged surface regions. The *dark green spheres* (positioned on atom C_ζ of Arg and C_γ of Ile/Leu) mark low ΔG anchoring spots. *C*, *surface representation* of the FXYD1 helical segment 60–70 *colored* according to its electrostatic potential. Compared with *A* and *B*, the helix is rotated by ~90° along its axis to show its amphipathic character.

phomimetic mutants (S68E, S63E, and S63E, S68E) behaved similarly in that there was no significant difference of $K_{0.5}$Na from the control (−FXYD1) and no dramatic dependence of $K_{0.5}{}^{Na}$ on the concentration of DOPS in the membrane. Especially in the range of 0–10 mol % DOPS, the variation of $K_{0.5}$Na is on the order of 10% or less. In short, either phosphorylation at Ser-68 or the phosphomimetic mutants cancels the effects of the wild-type FXYD1, so that no significant differences in the $K_{0.5}$Na values were observed between any of the FXYD1 forms. This behavior corresponds to what was observed for $\alpha 1\beta 1$-phospho-FXYD1 complexes in proteoliposomes made with excess DOPS (≥10 mol %), which leads to a membrane with a considerable negative surface charge (24).

Molecular Docking of a Cytoplasmic Helix of FXYD1—The Na,K-ATPase in complex with the transmembrane helix of FXYD2 (Protein Data Bank code 3kdp) (11) was used to construct a model that also includes the C-terminal H4 helix of FXYD1. In a first step, the transmembrane helix in the free FXYD1 structure (*yellow*), determined by NMR spectroscopy in SDS micelles (Protein Data Bank code 2jo1) (10) was superimposed onto the corresponding transmembrane segment in the Na,K-ATPase/FXYD2 complex by optimizing the match of Cα atoms of residues 25–45. Fig. 7*A* shows the superposition of free FXYD1 and the complex of Na,K-ATPase and the FXYD2 transmembrane helix (*green*). The H4 helix of the superposed FXYD1 is located near the transmembrane region of Na,K-ATPase, with only minor interactions (Fig. 7*A*). This position cannot explain, for example, the effects of phosphorylation of Ser-63 and Ser-68 on function, making it clear that in the real $\alpha_1\beta_1$FXYD1 complex, the H4 helix must be located differently and should be repositioned in the model. The best docking model for the H4 helix (residues 60–70) was obtained as described under "Methods," and, as seen in Fig. 7*A*, the H4 helix (*green*) is located in a groove between the Na,K-ATPase domains N and P. The GEH score is higher by 2σ than the next best model, which is also located in the same groove. The distance between the N terminus of the docked H4 helix docked segment, residues 60–70, and the C terminus of segment 13–39 of FXYD2 is 37 Å, a distance that can be spanned by 21 amino acids, making this position of the H4 helix feasible. The amino acids of segment 60–70 form an amphipathic helix with a strongly positively charged face and a hydrophobic face on the opposite side (Fig. 7*C*), which makes numerous electrostatic and hydrophobic interactions with the α subunit, respectively (Fig. 7*B*). Further support of this docking model was obtained by calculating preferred binding locations (anchoring spots) for arginine, isoleucine, and leucine on the surface of Na,K-ATPase, using ANCHORSmap. This independent computational approach identified anchoring spots that correspond well to the contacts made by Arg-61, Arg-65, Ile-64, and Leu-67 of helix 60–70 (Fig. 7*B, dark green spheres*).

Fig. 8*A* presents details of the cytoplasmic helix of FXYD1 bound to the cytoplasmic domain in the E_2 conformation (*gray ribbon*). This specific arrangement emphasizes direct electrostatic interactions of the four arginine residues with negatively charged residues (Arg-61 with Glu-392, Arg-65 with Glu-392

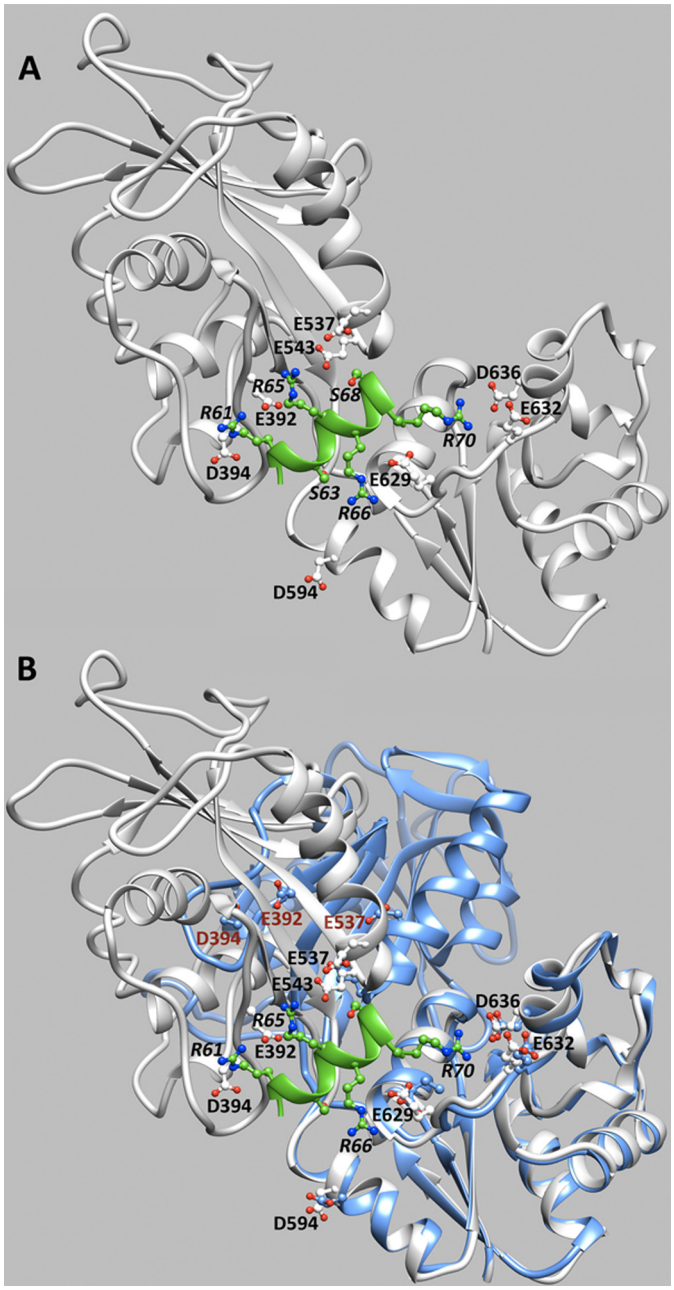

FIGURE 8. **Predicted location of the bound cytoplasmic H4 helix of FXYD1 in E_2 and E_1 conformations.** *A*, the four arginine residues in FXYD1 segment 60–70 (*green*; residues are *labeled* in *italic type*) can make numerous direct and indirect electrostatic interactions with the negative aspartate and glutamate residues presented in the E_2 conformation (Arg-61 with Glu-392, Arg-65 with Glu-392 and Glu-537, Arg-66 with Glu-629, and Arg-70 with Glu-632). *B*, the superposition of the P domain in the E_1 conformation (*blue*) and in the E_2 conformation (*light gray*) highlights the large motion of the N domain. The negative residues that interact in the E_2 conformation with the FXYD1 arginine side chains are shown as *ball-and-stick representations* and *labeled* in *black*. The corresponding negative residues in the E_1 conformation are *labeled* in *dark red*, showing that the motion of the N domain causes loss of the interactions with FXYD1 Arg-61 and Arg-65.

and Glu-537, Arg-66 with Glu-629, and Arg-70 with Asp-636). Residues Asp-394, Glu-543, Asp-594, and Glu-632 further strengthen the negative environment of the proposed Na,K-ATPase binding site and may contribute additionally to FXYD1 binding via indirect interactions facilitated by the solvent. Notably, Ser-63 and Ser-68, phosphorylation of which regulates the functional effects of FXYD1, point toward negatively charged surface regions of Na,K-ATPase (Figs. 7*B* and 8*A*). Thus, Ser-68 is located close to the strongly negative surface patch formed by the side chains of Glu-392, Glu-537, and Glu-543. Ser-63 is located close to a mildly negative region formed by the side chain of Asp-594 and the backbone carbonyl atoms of Gly-623, Val-624, and Pro-593. Replacement of each of these residues with glutamic acid and a local optimization of the position of the mutated segment 60–70 resulted in practically unchanged geometric and hydrophobic complementarity scores and significantly reduced electrostatic complementarity scores that led to a drop of 1.4σ in the GEH score. Replacement of both Ser-63 and Ser-68 with glutamic acid led to a drop of 2.5σ in the GEH score. Fig. 8*B* represents a superposition of the P domain in the E_1 conformation (Protein Data Bank code 3wgu; *blue ribbon*) (46) and in the E_2 conformation, which reveals the large N domain movement that takes place during the E_2 to E_1 conformation transition. Due to this movement, some of the negatively charged residues (Asp-394, Glu-392, Glu-537, and Glu-543) that line the binding site for the H4 helix of FXYD1 in E_2 are displaced and can no longer interact with the FXYD1 helix. Thus, the predicted binding location of the H4 helix of FXYD1 in the groove between the N and P domains of the Na,K-ATPase is available only when Na,K-ATPase has adopted the E_2 conformation.

Discussion

Here we present a hypothesis to explain the mechanism of functional effects of FXYD1 and its structural interactions, based on the experiments with the pure recombinant proteins, as described here and in our previous publications (23, 24, 43). The effects of FXYD1 on steady-state Na,K-ATPase activity, and in particular on the conformational changes and Na^+ binding affinity, are explained in relation to the crystal structures of the Na,K-ATPase in E_1 and E_2 conformations. This leads to an integrated concept of the regulatory effects of FXYD1 in non-phosphorylated and phosphorylated states. The hypothesis is then compared with functional effects of FXYD1 observed in other intact cell systems, primarily *Xenopus* oocytes and cardiomyocytes.

As an experimental system, the detergent-solubilized purified human recombinant Na,K-ATPase is very useful for analysis of the detailed mechanistic and structural interactions of FXYD1 (23, 24, 43). Several factors are important. First, measurements are accurate due to the high purity of the preparations (Fig. 1). This avoids the necessity of subtracting background effects of other ATP-consuming or ion-transporting systems from the pump-mediated activities, unlike the situation with native cell preparations. Second, detection and detailed analysis of effects on conformational changes and cation binding and release is possible only with pure $\alpha\beta$ complexes, prepared with and without the FXYD proteins. Third, the observed effects of FXYD1 are reproducible due to experimental control of *in vitro* reconstitution of the $\alpha\beta$FXYD1 complex, ensuring that the stoichiometric ratio of bound FXYD/$\alpha\beta$ is maximal (shown in crystal structures and by native protein

mass spectrometry to equal 1:1).[6] Fourth, recognition of the stabilizing effects of FXYD1 has led to establishment of experimental conditions, namely the use of sufficiently high lipid concentrations in the enzyme preparations, that allow detection of the true kinetic effects of FXYD1. Finally, the fact that FXYD1 expressed in *E. coli* is fully unphosphorylated (43), in contrast to FXYD1 expressed in *P. pastoris*, which is at least 50% phosphorylated on Ser-68 (41), allows analysis of the true kinetic effects of the unphosphorylated FXYD1 and the phosphomimetic mutants used in this study.

Mechanism of Functional Effects and Structural Interactions of FXYD1

Below, we discuss the detailed mechanisms of two separate kinetic effects of FXYD1 and separate structural interactions.

E_2(2K)ATP → $E_1$3NaATP

FXYD1 slows the conformational transition E_2(2K)ATP → $E_1$3NaATP, an effect attributed to docking of the H4 cytoplasmic helix in the groove between N and P domains. The interactions of H4 are significantly weakened in S63E or S68E mutants (or FXYD1 phosphorylated on Ser-63 or Ser-68).

The stopped-flow experiments have been crucial for identification of the reaction step affected by FXYD1. They demonstrate that the Na^+-translocating part of the Post-Albers cycle (namely E_1P(3Na) → E_2P) is unaffected by FXYD1 (Tables 4 and 5), whereas the rate constant of E_2(2K)ATP → $E_1$3NaATP, the K^+-translocating half-cycle, was reduced 20–40% by the wild-type FXYD1 (Table 4). Because the E_2(2K)ATP → $E_1$3NaATP conformation transition is the rate-limiting reaction step of the Post-Albers cycle (47, 48) the 25–40% reduction in rate suffices to explain a FXYD1-mediated reduction of the turnover rate of about 25% (Tables 4 and 5). When this partial reaction was performed in non-physiological conditions, namely in the absence of ATP, FXYD1 had no effect. In this condition, the rate-limiting step of E_2(2K) → $E_1$3Na is about 70 times slower than in the presence of ATP (Table 5), a fact known for many years (49).

The structure of the Na,K-ATPase in the E_2 conformation together with the molecular modeling presented above provides a simple explanation for the different effects of FXYD1 on the conformational transition, with and without ATP. In the absence of ATP, the rate-limiting step of E_2(2K) → $E_1$3Na is thought to be dissociation of salt bridges, Glu-216 to Arg-544 between A and N and Glu-231 to Arg-685 between A and P domains (12, 50). ATP accelerates the rate of dissociation of these two salt bridges by competing with Glu-216 and Glu-231 for Arg-544 and Arg-685, which are direct ATP binding residues, and thus strongly accelerates the rate of the reaction sequence E_2(2K) → $E_1$3Na. In the presence of ATP, the reaction sequence E_2(2K)ATP → $E_1$3NaATP is no longer limited by the dissociation of the Glu-216 to Arg-544 and Glu-231 to Arg-685 salt bridges, and interaction of the FXYD1 with the N domain residues (primarily Arg-61 with Glu-392 and Arg-65 with Glu-392 and Glu-537) can slow the rate of the E_2(2K)ATP → $E_1$3NaATP by interfering with the association of the N and P domains. In contrast, in the absence of ATP, the characteristic time of FXYD1 interaction with its binding site is significantly shorter compared with the rearrangement of the N, P, and A domains due to the slow dissociation of the Glu-216 to Arg-544 and Glu-231 to Arg-685 salt bridges, and thus FXYD1 no longer reduces the rate of E_2(2K) → $E_1$3Na (Table 5).

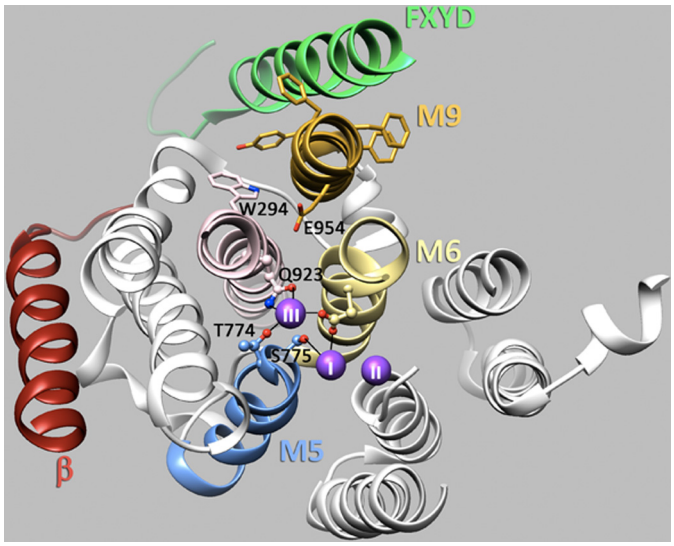

FIGURE 9. **An interaction of the FXYD1 transmembrane segment with Na^+ binding site III?** The view is from the cytoplasm. The transmembrane helix of FXYD is shown in *green*, βTM is shown in *red*, and αTM helices are depicted in *light gray*. Highlighted are αM5, M6, M8, and M9 in blue, yellow, pink, and gold, respectively. *Magenta spheres* represent Na^+ ions. Hydrophobic residues of M9 forming a groove to accommodate the FXYD helix are shown in *stick representation*. Glu-954 in M9 is highlighted. A potential salt bridge with Trp-924 of M8 is indicated. Residues from M5, M6, and M8 coordinating the Na^+ site III (E_1Na3) are depicted in a *ball-and-stick representation*.

In a previous publication (24), we have presented a model of interaction of the Arg-65, Arg-66, and Arg-70 of the H4 helix with surface charges of the N domain (Glu-544, Glu-399), which may appear to differ from the current model that predicts a position between the N and P domains and includes both electrostatic and hydrophobic interactions. The model in Ref. 24 was obtained by a molecular dynamics simulation over 7 ns, which cannot, of course, predict a time-independent equilibrium position of the H4 helix, as in the present model in Figs. 7 and 8. Nor can a molecular dynamics simulation over 7 ns explain the effect of the FXYD1 on the E_2(2K)ATP → $E_1$3NaATP conformational transition over a 6-order of magnitude slower time scale ($t_{0.5}$ ~5–10 ms at 37 °C). A likely interpretation is that the molecular dynamics simulation has identified an initial encounter complex in a local energy minimum on the surface of the N domain, and, over time (milliseconds), the helix rearranges to the equilibrium position between the N and P domains, which is more specific. Thus, in reality, the two models are not contradictory but complement each other in pointing to (*a*) an initial encounter complex and (*b*) the equilibrium binding location in the E_2 conformation and the N domain as a main interaction site of the H4 helix and also mobility of the H4 helix.

The effects of phosphorylated wild-type FXYD1 or phosphomimetic mutants to abolish the kinetic effects of the wild-type FXYD1 on V_{max} and $K_{0.5}$Na are explained readily on the assumption that binding of the C terminus H4 helix carrying

[6] M. Habeck, M. Sharon, and S. J. D. Karlish, unpublished work.

negatively charged side chains at Ser-63 or Ser-68 is weakened, as predicted by the modeling. Because the H4 helix is also mobile, it can dissociate from the groove between the N and P domains, so its effect on the conformational change is abolished. Thus, the findings with the phosphomimetic mutant strongly indicate that the positive charge present on the arginine residues (Arg-61, Arg-65, Arg-66, Arg-70, and possibly Arg-71 and Arg-72, which are not included in the docking model) of the H4 helix of FXYD1 cause the reduction of the activity of the Na,K-ATPase (Figs. 2 and 5).

This explanation also fits very well with our recent demonstration that electrostatic effects play a major role in this mechanism (24). When the predominantly positively charged and highly mobile C-terminal end of wild-type FXYD1 is attracted by and subsequently immobilized on the negatively charged surface of DOPS-rich vesicle membranes, the modifying effect of FXYD1 on $K_{0.5}$Na disappears. In the case of the phosphorylated wild-type FXYD1 and the phosphomimetic mutants that carry negatively charged side chains on the C terminus, the effect of the negative membrane charges is abolished. These findings with DOPS-rich vesicles, described here and in our recent paper (24), support the notion that the positively charged C-terminal domain is highly mobile. It may bind temporarily to a negatively charged patch of the cytoplasmic domain of the Na,K-ATPase, and either upon introduction of negative charges on FXYD1 by phosphorylation or in the presence of excess negative charge in the membrane surface, the helix dissociates, and its functional effect is lost.

Na^+ Site III

FXYD1 selectively increases the binding affinity of Na^+ ions, with no effect on K/Rb binding (43). This indicates that FXYD1 modulates Na^+ binding only at the third Na^+-specific site III. This effect is not altered by phosphorylation of Ser-68. It is attributable to an interaction of the transmembrane domain of FXYD1. In Na,K-ATPase activity assays, it is detected as the lower $K_{0.5}$Na for Na,K-ATPase activity in the phosphomimetic mutants compared with the control. In initial studies using FXYD1 expressed in *P. pastoris*, we observed that FXYD1 raises the apparent V_{max} of the Na,K-ATPase activity and reduces $K_{0.5}$Na (*i.e.* the exact opposite of the present observations). With our current understanding, the apparent increase in V_{max} is explained easily by stabilization of the partially inactivated control (22, 23), and the reduced $K_{0.5}$Na is explained by the fact that FXYD1 expressed in the yeast is at least 50% phosphorylated at Ser-68 and phosphorylation at Ser-63 was also possible (but unknown) (41). Thus, it is now evident that the functional effects of the FXYD1 expressed in *P. pastoris* should be compared with those of the S68E (or S63E,S68E) mutants.

A likely mechanism of increased Na^+ site III affinity can be proposed from the structure of the pump in the $E_1$3Na bound conformation (Fig. 9). The transmembrane segment of the FXYD protein is bound to TM9 of the α subunit, and Glu-954 in TM9 points inward toward M8 (and may interact with Trp-824) and Na^+ site III. It was shown previously that mutations of Glu-954 selectively reduce extracellular Na^+ (but not K^+) binding affinity (51). Thus, one can propose that binding of the FXYD1 protein to TM9 affects the interaction of Glu-954 with M8 and thus indirectly affects (moderately raises) binding affinity of Na^+ to site III. By comparison with the Na^+ site III in E_1, the two potassium sites in the E_2 conformation do not interact directly with M8, and thus FXYD1 should not affect potassium binding, as found experimentally.

It is important to note that the kinetic effects of FXYD1 on the steady-state Na,K-ATPase activity (Tables 2 and 3) can be presumed to reflect the sum of the individual effects. Upon binding of unphosphorylated FXYD1, the V_{max} and turnover rate are reduced, and, in theory, the poise toward E_2(2K) and away from E_1 should also be secondarily associated with a raised $K_{0.5}$Na. The increased $K_{0.5}$Na seen in Na,K-ATPase activity assays should then represent the balance of increased $K_{0.5}$Na associated with the slower turnover rate and the decreased $K_{0.5}$Na that reflects the increased affinity for Na^+ site III. Upon phosphorylation at Ser-68 or with the phosphomimetic mutants, the inhibition of turnover is relieved, and now the increased Na^+ site binding affinity of site III becomes apparent as a reduced $K_{0.5}$Na compared with control. As illustrated by the calculation under "Results," the combination of the two effects should make for optimal efficiency of regulation in physiological conditions of limiting cytoplasmic Na^+ concentrations.

Comparison with Effects of FXYD1 Observed in Whole Cells

The most comprehensive studies to date on effects of FXYD1 have been carried out using *Xenopus* oocytes transfected with FXYD1, cultured mammalian cells, or isolated cardiac myocytes of wild-type or FXYD1 knock-out mice (15–20, 52, 53) (reviewed recently in Ref. 21). The overall conclusion is that unphosphorylated FXYD1 inhibits the Na,K-pump *in vivo*, and activators of PKA or PKC induce phosphorylation of FXYD1 at Ser-68 or Ser-63, respectively, and relieve the inhibition. It is suggested that with unphosphorylated FXYD1, the V_{max} is depressed and $K_{0.5}$Na is elevated compared with phosphorylated FXYD1 or with FXYD1 knock-out mice, with an elevated V_{max} and reduced $K_{0.5}$Na. All effects are assumed to be mediated by the H4 cytoplasmic helix of FXYD1 (see Fig. 2 in Ref. 21). Although studies in intact cells more closely reflect the real physiological situation, there are significant inconsistencies in reported effects of FXYD1 for different cell types or isoforms. As pointed out in Ref. 21, different studies show that FXYD1 raises $K_{0.5}{}^{Na}$ (15–17, 19, 20, 41) or decreases V_{max} (53–56) or affects both parameters (18, 57). Two sets of studies suffice as illustrations. Expression of wild-type FXYD1 in *Xenopus* oocytes, together with either $\alpha1\beta1$ or $\alpha2\beta1$ isoforms, significantly raises $K_{0.5}$Na (and slightly raises $K_{0.5}$K) for activating the pump-mediated current of both isoforms but has no effect on the V_{max} (19). Subsequently it was found that PKA- or PKC-mediated phosphorylation of FXYD1 at either Ser-68 or Ser-63 reduces the $K_{0.5}$Na of $\alpha1\beta1$ with no effect on V_{max}, whereas PKC-stimulated phosphorylation of FXYD raises the V_{max} and turnover number of $\alpha2\beta1$ (but $K_{0.5}$Na of $\alpha2\beta1$ was not determined) (18). As a second example, experiments using cardiac myocytes from wild-type and FXYD1 knock-out mice have shown unequivocally that stimulation of PKA or PKC in wild-type cardiomyocytes leads to stimulation (or deinhibition) of the Na,K-pump associated with phosphorylation of FXYD1 at Ser-68 or Ser-63, respectively, and these effects are not seen in

the FXYD1 knock-out animals (16). PKA-dependent phosphorylation was associated with a decreased $K_{0.5}$Na for both $\alpha1\beta1$ and $\alpha2\beta1$ with no effect on V_{max}, whereas PKC-dependent phosphorylation was associated with a decreased $K_{0.5}$Na for both $\alpha1\beta1$ and $\alpha2\beta1$ and no effect on V_{max} of $\alpha1\beta1$ but an increased V_{max} of $\alpha2\beta1$ (15).

Considering the rather small but highly significant effects of the FXYD1 variants on purified human $\alpha1\beta$ and $\alpha2\beta1$ isoforms, the discrepancies in reported effects on V_{max} and $K_{0.5}$Na in whole cell studies pointed out previously (21) may be attributable to lower accuracy in the measurement of pump-mediated currents, different degrees of endogenous phosphorylation of FXYD1, and lower than 1:1 stoichiometry of FXYD1/$\alpha\beta$. For example, the reported experimental variation in measurement of Na,K-pump currents in most whole cell studies is $\geq$20%, making it difficult to detect significant differences of V_{max} for either $\alpha1\beta1$ (25%) or $\alpha2\beta1$ (15%), as observed here.

Conclusion

The effects of FXYD1 and the phosphomimetic mutants on the steady-state Na,K-ATPase activities observed here using the purified proteins are largely consistent with the information from whole cell experiments. The limitation of the unphysiological conditions of work with the purified proteins is offset by the higher accuracy and reproducibility of the measurements and the possibility to define the detailed mechanism of action, using the RH421 dye. This has added to the physiological data in revealing two separate molecular effects of FXYD1: (*a*) slowing of E_2(2K)ATP $\rightarrow$ $E_1$3NaATP and (*b*) increased affinity for Na^+ at selective site III. Potentially, detailed comparisons of effects of wild-type FXYD1 and S68E or S63E mutants on the E_2(2K)ATP $\rightarrow$ $E_1$3NaATP transition, for both $\alpha1\beta1$ and $\alpha2\beta1$, could clarify the somewhat different effects of PKA (Ser-68) and PKC (Ser-63) phosphorylation on $\alpha1\beta1$ and $\alpha2\beta1$ described in whole cells (15, 18). Thus, overall, the different experimental approaches using whole cells and purified proteins can provide complementary information and a more complete and detailed picture of the regulatory mechanism of FXYD1.

Author Contributions—N. K. M., M. H., C. K., and H. H. performed the experiments. Y. P. produced the wild-type FXYD1 and mutants. M. E. performed the molecular modeling. H. J. A. and S. J. D. K. conceived and planned the experiments, coordinated the study, and wrote the paper.

References

1. Blanco, G., and Mercer, R. W. (1998) Isozymes of the Na-K-ATPase: heterogeneity in structure, diversity in function. *Am. J. Physiol.* **275,** F633–F650
2. Cornelius, F., and Mahmmoud, Y. A. (2003) Functional modulation of the sodium pump: the regulatory proteins "Fixit". *News Physiol. Sci.* **18,** 119–124
3. Garty, H., and Karlish, S. J. (2006) Role of FXYD proteins in ion transport. *Annu. Rev. Physiol.* **68,** 431–459
4. Geering, K. (2006) FXYD proteins: new regulators of Na-K-ATPase. *Am. J. Physiol. Renal Physiol.* **290,** F241–F250
5. Sweadner, K. J., and Rael, E. (2000) The FXYD gene family of small ion transport regulators or channels: cDNA sequence, protein signature sequence, and expression. *Genomics* **68,** 41–56
6. Palmer, C. J., Scott, B. T., and Jones, L. R. (1991) Purification and complete sequence determination of the major plasma membrane substrate for cAMP-dependent protein kinase and protein kinase C in myocardium. *J. Biol. Chem.* **266,** 11126–11130
7. Presti, C. F., Scott, B. T., and Jones, L. R. (1985) Identification of an endogenous protein kinase C activity and its intrinsic 15-kilodalton substrate in purified canine cardiac sarcolemmal vesicles. *J. Biol. Chem.* **260,** 13879–13889
8. Feschenko, M. S., Donnet, C., Wetzel, R. K., Asinovski, N. K., Jones, L. R., and Sweadner, K. J. (2003) Phospholemman, a single-span membrane protein, is an accessory protein of Na,K-ATPase in cerebellum and choroid plexus. *J. Neurosci.* **23,** 2161–2169
9. Floyd, R. V., Wray, S., Martín-Vasallo, P., and Mobasheri, A. (2010) Differential cellular expression of FXYD1 (phospholemman) and FXYD2 (γ subunit of Na,K-ATPase) in normal human tissues: a study using high density human tissue microarrays. *Ann. Anat.* **192,** 7–16
10. Teriete, P., Franzin, C. M., Choi, J., and Marassi, F. M. (2007) Structure of the Na,K-ATPase regulatory protein FXYD1 in micelles. *Biochemistry* **46,** 6774–6783
11. Morth, J. P., Pedersen, B. P., Toustrup-Jensen, M. S., Sørensen, T. L., Petersen, J., Andersen, J. P., Vilsen, B., and Nissen, P. (2007) Crystal structure of the sodium-potassium pump. *Nature* **450,** 1043–1049
12. Shinoda, T., Ogawa, H., Cornelius, F., and Toyoshima, C. (2009) Crystal structure of the sodium-potassium pump at 2.4 Å resolution. *Nature* **459,** 446–450
13. Walaas, S. I., Horn, R. S., Albert, K. A., Adler, A., and Walaas, O. (1988) Phosphorylation of multiple sites in a 15,000 dalton proteolipid from rat skeletal muscle sarcolemma, catalyzed by adenosine 3′,5′-monophosphate-dependent and calcium/phospholipid-dependent protein kinases. *Biochim. Biophys. Acta* **968,** 127–137
14. Walaas, S. I., Czernik, A. J., Olstad, O. K., Sletten, K., and Walaas, O. (1994) Protein kinase C and cyclic AMP-dependent protein kinase phosphorylate phospholemman, an insulin and adrenaline-regulated membrane phosphoprotein, at specific sites in the carboxy terminal domain. *Biochem. J.* **304,** 635–640
15. Bossuyt, J., Despa, S., Han, F., Hou, Z., Robia, S. L., Lingrel, J. B, and Bers, D. M. (2009) Isoform specificity of the Na/K-ATPase association and regulation by phospholemman. *J. Biol. Chem.* **284,** 26749–26757
16. Despa, S., Bossuyt, J., Han, F., Ginsburg, K. S., Jia, L. G., Kutchai, H., Tucker, A. L., and Bers, D. M. (2005) Phospholemman-phosphorylation mediates the beta-adrenergic effects on Na/K pump function in cardiac myocytes. *Circ. Res.* **97,** 252–259
17. Han, F., Tucker, A. L., Lingrel, J. B, Despa, S., and Bers, D. M. (2009) Extracellular potassium dependence of the Na^+-K^+-ATPase in cardiac myocytes: isoform specificity and effect of phospholemman. *Am. J. Physiol. Cell Physiol.* **297,** C699–C705
18. Bibert, S., Roy, S., Schaer, D., Horisberger, J. D., and Geering, K. (2008) Phosphorylation of phospholemman (FXYD1) by protein kinases A and C modulates distinct Na,K-ATPase isozymes. *J. Biol. Chem.* **283,** 476–486
19. Crambert, G., Fuzesi, M., Garty, H., Karlish, S., and Geering, K. (2002) Phospholemman (FXYD1) associates with Na,K-ATPase and regulates its transport properties. *Proc. Natl. Acad. Sci. U.S.A.* **99,** 11476–11481
20. Han, F., Bossuyt, J., Martin, J. L., Despa, S., and Bers, D. M. (2010) Role of phospholemman phosphorylation sites in mediating kinase-dependent regulation of the Na^+-K^+-ATPase. *Am. J. Physiol. Cell Physiol.* **299,** C1363–C1369
21. Pavlovic, D., Fuller, W., and Shattock, M. J. (2013) Novel regulation of cardiac Na pump via phospholemman. *J. Mol. Cell. Cardiol.* **61,** 83–93
22. Lifshitz, Y., Petrovich, E., Haviv, H., Goldshleger, R., Tal, D. M., Garty, H., and Karlish, S. J. (2007) Purification of the human $\alpha2$ isoform of Na,K-ATPase expressed in *Pichia pastoris*: stabilization by lipids and FXYD1. *Biochemistry* **46,** 14937–14950
23. Mishra, N. K., Peleg, Y., Cirri, E., Belogus, T., Lifshitz, Y., Voelker, D. R., Apell, H. J., Garty, H., and Karlish, S. J. (2011) FXYD proteins stabilize Na,K-ATPase: amplification of specific phosphatidylserine-protein interactions. *J. Biol. Chem.* **286,** 9699–9712
24. Cirri, E., Kirchner, C., Becker, S., Katz, A., Karlish, S. J., and Apell, H. J. (2013) Surface charges of the membrane crucially affect regulation of

Na,K-ATPase by phospholemman (FXYD1). *J. Membr. Biol.* **246,** 967–979
25. Habeck, M., Cirri, E., Katz, A., Karlish, S. J., and Apell, H. J. (2009) Investigation of electrogenic partial reactions in detergent-solubilized Na,K-ATPase. *Biochemistry* **48,** 9147–9155
26. Apell, H. J., and Bersch, B. (1987) Oxonol VI as an optical indicator for membrane potentials in lipid vesicles. *Biochim. Biophys. Acta* **903,** 480–494
27. Habeck, M., Haviv, H., Katz, A., Kapri-Pardes, E., Ayciriex, S., Shevchenko, A., Ogawa, H., Toyoshima, C., and Karlish, S. J. (2015) Stimulation, inhibition, or stabilization of Na,K-ATPase caused by specific lipid interactions at distinct sites. *J. Biol. Chem.* **290,** 4829–4842
28. Haviv, H., Cohen, E., Lifshitz, Y., Tal, D. M., Goldshleger, R., and Karlish, S. J. (2007) Stabilization of Na^+,K^+-ATPase purified from *Pichia pastoris* membranes by specific interactions with lipids. *Biochemistry* **46,** 12855–12867
29. Haviv, H., Habeck, M., Kanai, R., Toyoshima, C., and Karlish, S. J. (2013) Neutral phospholipids stimulate Na,K-ATPase activity: a specific lipid-protein interaction. *J. Biol. Chem.* **288,** 10073–10081
30. Kapri-Pardes, E., Katz, A., Haviv, H., Mahmmoud, Y., Ilan, M., Khalfin-Penigel, I., Carmeli, S., Yarden, O., Karlish, S. J. (2011) Stabilization of the α2 isoform of Na,K-ATPase by mutations in a phospholipid binding pocket. *J. Biol. Chem.* **286,** 42888–42899
31. Erijman, A., Dantes, A., Bernheim, R., Shifman, J. M., and Peleg, Y. (2011) Transfer-PCR (TPCR): a highway for DNA cloning and protein engineering. *J. Struct. Biol.* **175,** 171–177
32. Erijman, A., Shifman, J. M., and Peleg, Y. (2014) A single-tube assembly of DNA using the transfer-PCR (TPCR) platform. *Methods Mol. Biol.* **1116,** 89–101
33. Berchanski, A., Shapira, B., and Eisenstein, M. (2004) Hydrophobic complementarity in protein-protein docking. *Proteins* **56,** 130–142
34. Heifetz, A., Katchalski-Katzir, E., and Eisenstein, M. (2002) Electrostatics in protein-protein docking. *Protein Sci.* **11,** 571–587
35. Katchalski-Katzir, E., Shariv, I., Eisenstein, M., Friesem, A. A., Aflalo, C., Vakser, I. A. (1992) Molecular surface recognition: determination of geometric fit between proteins and their ligands by correlation techniques. *Proc. Natl. Acad. Sci. U.S.A.* **89,** 2195–2199
36. Heifetz, A., and Eisenstein, M. (2003) Effect of local shape modifications of molecular surfaces on rigid-body protein-protein docking. *Protein Eng.* **16,** 179–185
37. Kowalsman, N., and Eisenstein, M. (2007) Inherent limitations in protein-protein docking procedures. *Bioinformatics* **23,** 421–426
38. Kowalsman, N., and Eisenstein, M. (2009) Combining interface core and whole interface descriptors in postscan processing of protein-protein docking models. *Proteins* **77,** 297–318
39. Pettersen, E. F., Goddard, T. D., Huang, C. C., Couch, G. S., Greenblatt, D. M., Meng, E. C., and Ferrin, T. E. (2004) UCSF Chimera: a visualization system for exploratory research and analysis. *J. Comput. Chem.* **25,** 1605–1612
40. Ben-Shimon, A., and Eisenstein, M. (2010) Computational mapping of anchoring spots on protein surfaces. *J. Mol. Biol.* **402,** 259–277
41. Lifshitz, Y., Lindzen, M., Garty, H., and Karlish, S. J. (2006) Functional interactions of phospholemman (PLM) (FXYD1) with Na^+,K^+-ATPase: purification of α1/β1/PLM complexes expressed in *Pichia pastoris*. *J. Biol. Chem.* **281,** 15790–15799
42. Bühler, R., Stürmer, W., Apell, H. J., and Läuger, P. (1991) Charge translocation by the Na,K-pump: I. Kinetics of local field changes studied by time-resolved fluorescence measurements. *J. Membr. Biol.* **121,** 141–161
43. Cirri, E., Katz, A., Mishra, N. K., Belogus, T., Lifshitz, Y., Garty, H., Karlish, S. J., and Apell, H. J. (2011) Phospholemman (FXYD1) raises the affinity of the human α1β1 isoform of Na,K-ATPase for Na ions. *Biochemistry* **50,** 3736–3748
44. Cornelius, F. (1999) Rate determination in phosphorylation of shark rectal Na,K-ATPase by ATP: temperature sensitivity and effects of ADP. *Biophys. J.* **77,** 934–942
45. Karlish, S. J. (1980) Characterization of conformational changes in (Na,K) ATPase labeled with fluorescein at the active site. *J. Bioenerg. Biomembr.* **12,** 111–136
46. Kanai, R., Ogawa, H., Vilsen, B., Cornelius, F., and Toyoshima, C. (2013) Crystal structure of a Na^+-bound Na^+,K^+-ATPase preceding the E1P state. *Nature* **502,** 201–206
47. Karlish, S. J., and Yates, D. W. (1978) Tryptophan fluorescence of (Na^++K^+)-ATPase as a tool for study of the enzyme mechanism. *Biochim. Biophys. Acta* **527,** 115–130
48. Clarke, R. J., Humphrey, P. A., Lüpfert, C., Apell, H. J., and Cornelius, F. (2003) Kinetic investigations of the mechanism of the rate-determining step of the Na^+,K^+-ATPase pump cycle. *Ann. N.Y. Acad. Sci.* **986,** 159–162
49. Karlish, S. J., Yates, D. W., and Glynn, I. M. (1978) Conformational transitions between Na^+-bound and K^+-bound forms of (Na^++K^+)-ATPase, studied with formycin nucleotides. *Biochim. Biophys. Acta* **525,** 252–264
50. Belogus, T., Haviv, H., and Karlish, S. J. (2009) Neutralization of the charge on Asp^{369} of Na^+,K^+-ATPase triggers E1 [dharrow] E2 conformational changes. *J. Biol. Chem.* **284,** 31038–31051
51. Li, C., Capendeguy, O., Geering, K., and Horisberger, J. D. (2005) A third Na^+-binding site in the sodium pump. *Proc. Natl. Acad. Sci. U.S.A.* **102,** 12706–12711
52. Bossuyt, J., *et al.* (2005) Phospholemman phosphorylation mediates the beta-adrenergic effects on Na/K ATPase function in ventricular myocytes. *Biophys. J.* **88,** 9a
53. Pavlović, D., Fuller, W., and Shattock, M. J. (2007) The intracellular region of FXYD1 is sufficient to regulate cardiac Na/K ATPase. *FASEB J.* **21,** 1539–1546
54. Fuller, W., Howie, J., McLatchie, L. M., Weber, R. J., Hastie, C. J., Burness, K., Pavlovic, D., and Shattock, M. J. (2009) FXYD1 phosphorylation *in vitro* and in adult rat cardiac myocytes: threonine 69 is a novel substrate for protein kinase C. *Am. J. Physiol. Cell Physiol.* **296,** C1346–C1355
55. Silverman, B., Fuller, W., Eaton, P., Deng, J., Moorman, J. R., Cheung, J. Y., James, A. F., and Shattock, M. J. (2005) Serine 68 phosphorylation of phospholemman: acute isoform-specific activation of cardiac Na/K ATPase. *Cardiovasc. Res.* **65,** 93–103
56. Zhang, X. Q., Moorman, J. R., Ahlers, B. A., Carl, L. L., Lake, D. E., Song, J., Mounsey, J. P., Tucker, A. L., Chan, Y. M., Rothblum, L. I., Stahl, R. C., Carey, D. J., and Cheung, J. Y. (2006) Phospholemman overexpression inhibits Na^+-K^+-ATPase in adult rat cardiac myocytes: relevance to decreased Na^+ pump activity in postinfarction myocytes. *J. Appl. Physiol.* **100,** 212–220
57. Han, F., Bossuyt, J., Despa, S., Tucker, A. L., and Bers, D. M. (2006) Phospholemman phosphorylation mediates the protein kinase C-dependent effects on Na^+/K^+ pump function in cardiac myocytes. *Circ. Res.* **99,** 1376–1383
58. Jørgensen, P. L. (1988) Purification of Na^+,K^+-ATPase: enzyme sources, preparative problems, and preparation from mammalian kidney. *Methods Enzymol.* **156,** 29–43